J. Indian Inst. Sci., Jan.–Feb. 1996, 76, 73–91.

On radial film flow on a horizontal surface and the circular hydraulic jump

JAYWANT H. ARAKERI AND K. P. ACHUTH RAO
Department of Mechanical Engineering, Indian Institute of Science, Bangalore-560 012, India.

Received on October 15, 1995.

Abstract

This paper deals with the radially flowing film produced by a vertical liquid jet impinging on a horizontal surface. Typically, circular hydraulic jump is formed at some radius. A new integral method to calculate the film flow is proposed. Flow visualization pictures and film thickness measurements for a range of flow rates are presented. A newly discovered phenomenon of surface wave-induced transition is discussed.

Keywords: Film flow, circular hydraulic jump, transition to turbulence, waves in film flow.

1. Introduction

Film flows have important applications in the industry and are also of interest from a fundamental viewpoint. Perhaps the simplest film flow is the one obtained by the impingement of a liquid jet on a horizontal surface—a common occurrence in the kitchen sink. In spite of its apparent simplicity a rich range of phenomena involving waves, hydraulic jump, separation, transition and turbulence are observed. Inertia, gravity, viscosity and surface tension all play a role. There is extensive literature on this subject involving both analysis and experiments.

The flow configuration is shown in Fig. 1. A circular liquid jet impinging vertically on a horizontal surface produces a radially spreading film flow. If the flow rate is 'large' (the meaning of large will become clear later on) the film is thin and the flow is supercritical a short distance away from the point of impingement; for the cases of interest in this paper the film thickness is typically a fraction of a millimeter. A circular hydraulic jump may be formed at some distance, x_j. The parameters of the problem are the jet flow rate Q, the jet radius at the point of impingement, a, fluid kinematic viscosity, ν, and surface tension, σ, acceleration due to gravity, the plate radius R_p, and the jet velocity, $U_j = Q/\pi a^2$. In some cases, a barrier has been used in which case the barrier height will be an additional parameter. We may usefully demarcate the flow into the following regions (see Fig. 1):

(I) stagnation region;
(II) developing region where the boundary layer is below the free surface and the velocity above the boundary layer is approximately equal to the jet velocity;

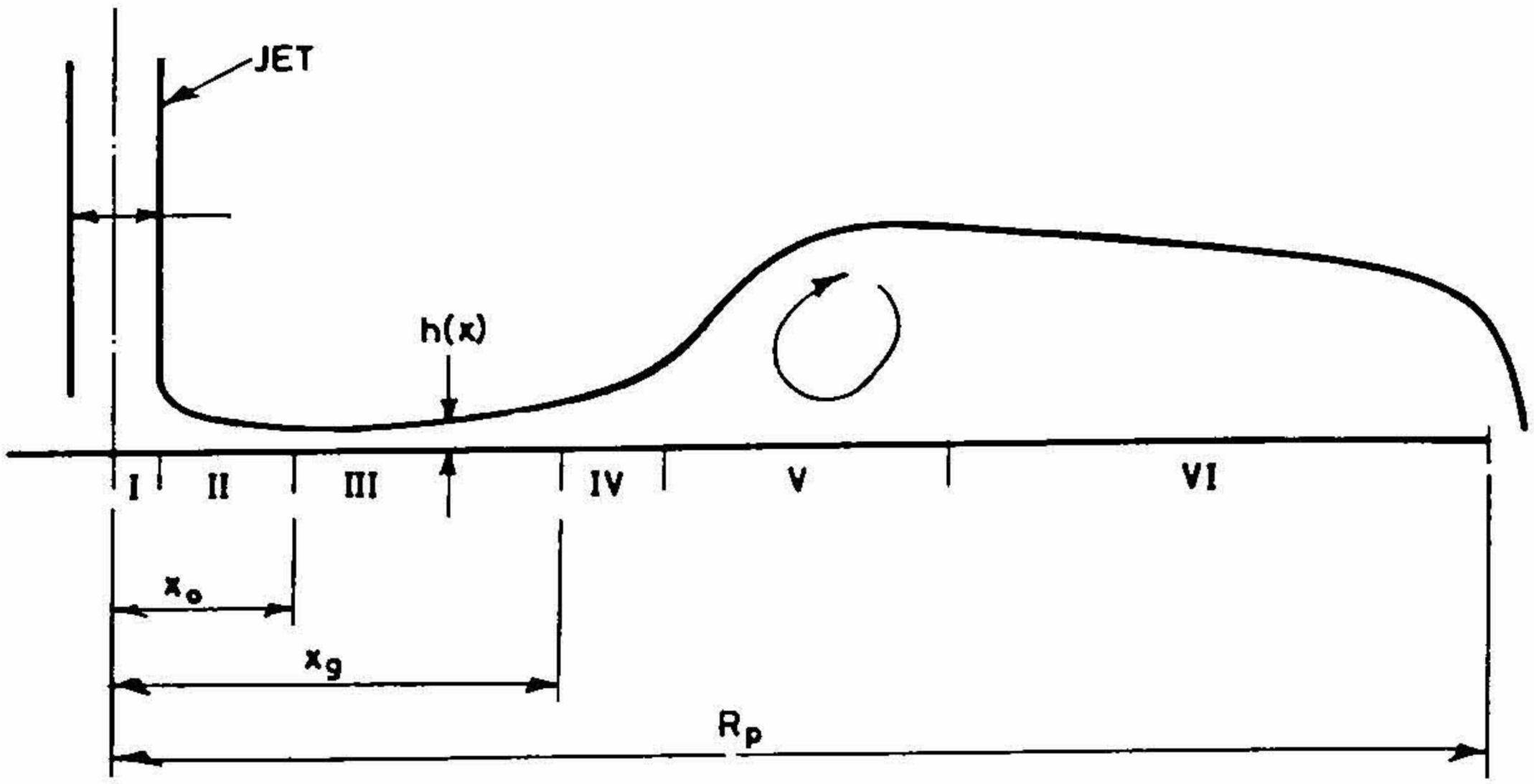

FIG. 1. Various regions in the radial film flow.

(III) developed region where viscous effects are felt up to the free surface; gravity is not important;
(IV) gravity effects are important and an adverse pressure gradient is present;
(V) the hydraulic jump region including the separation eddy;
(VI) flow downstream of the jump up to the edge of the plate $x = R_p$.

We note that viscous effects are felt up to the free surface downstream of region II. Upstream of the jump the flow is supercritical and sub-critical at the downstream. In regions IV, V and VI, the local Froude number is of order one and gravity is important. Not all regions may exist in a given case. If the plate radius is small enough a hydraulic jump will not exist; and, in some cases, region IV will not exist. The flow is essentially elliptic in that the edge of the plate determines the jump location and the flow downstream of the jump.

Various aspects of the flow have been studied and reported in the literature. A similarity solution of the boundary-layer equations in the developed region (III) and approximate solutions in regions I and II were given by Watson[1]. He obtained reasonable agreement between the jump location calculated from his solutions and the measured jump locations from his experiments. He used a barrier in his experiments and assumed that the flow height downstream of the jump is equal to the barrier height. Earlier Tani[2] recognised the existence of the region of adverse pressure gradient and postulated that the resulting separation causes the hydraulic jump. More recently, regions both upstream and downstream of the jump have been solved using essentially integral methods[3,4] or numerical solution of the full equations[5-7]. Bohr *et al.*[8] using novel scaling variables gave a relation for jump location for flows on plates of large radius. The boundary condition at the edge of the plate is of interest; critical flow (unity Froude number) or infinite

slope of the film has been used as edge condition. The jump condition due to Rayleigh[9], modified in various ways to account for the non-uniform velocity profiles and the finite jump length, has been used to patch the regions upstream and downstream of the jump.

Craik *et al.*[10] measured film thickness using an optical technique and studied the structure of the jump region. They noted that the waves downstream of the jump cannot be standing waves as the group velocity is larger than the phase velocity. Bowles and Smith[11] solved the region close to jump and compared their calculated profile to the one measured by Craik *et al.*[10] They showed that viscosity, gravity and surface tension are important in this region.

Azuma and his coworkers in a series of papers[12–16] have documented various regimes of the flow upstream of the jump. (They have done both types of experiments with flow on the upper or the lower surface. The only essential difference is that for flow on the upper surface, a hydraulic jump is obtained whereas for flow on the lower surface the thin film falls off due to gravity at some radial distance. Upstream of the jump and upstream of the 'fall off' the two flows are apparently the same). At certain flow rates they observe concentric waves; they term these roll waves as they believe them to be analogous to the roll waves observed on free surface flows on inclined planes. At still higher flow rates instability waves of the Tolmein–Schlichting type are observed which breakdown to turbulence. They show that linear stability analysis of the Watson's similarity profile can explain the observed instability waves and their breakdown; the critical Reynolds number of Watson's profile based on local free surface velocity and film thickness is about 450, lower than the critical Re for Blassius profile. From experimental data they obtain the critical jet Reynolds number ($= Q/\nu a$) to be 7.4×10^4. The transition point moves upstream with an increase in jet Reynolds number. The local Reynolds number goes down like the inverse of radial distance and we may expect relaminarization. Azuma *et al.*[12] do observe instability waves which decay and do not breakdown. They do not, however, report any observation of relaminarization.

2. Governing equations

Invoking the boundary-layer approximation the differential equations for steady, radial, axisymmetric film flow are :

$$\frac{\partial(ux)}{\partial x} + \frac{\partial(vx)}{\partial x} = 0 \tag{1}$$

and momentum,

$$u\frac{\partial u}{\partial x} + v\frac{\partial u}{\partial y} = \nu\frac{\partial^2 u}{\partial y^2} - g\frac{dh}{dx}. \tag{2}$$

Here, x is the radial coordinate and y, the coordinate normal to the plate surface; u and v are radial and normal components of velocity; and h, the film thickness. The term $-gdh/dx$ in eqn (2) comes from the y momentum equation, assuming pressure to be hydrostatic. The volume flux, Q, is constant at any section:

$$\int_0^h uxdy = \frac{Q}{2\pi} = q. \tag{3}$$

Integrating eqn (2) from $y = 0$ to $y = h$ and using Leibnitz rule we get the momentum integral equation,

$$\frac{1}{x}\frac{d}{dx}\int_0^h \left(u^2 x\right)dy = -\nu\left(\frac{\partial u}{\partial y}\right)_0 - g\frac{dh}{dx}h. \tag{4}$$

Integrating eqn (2) after multiplying by u we get the integral equation for mechanical energy.

$$\frac{d}{dx}\int_0^h \frac{\left(u^3 x\right)}{2}dy = -\nu\int_0^h \left(\frac{\partial u}{\partial y}\right)^2 dy - gq\frac{dh}{dx}. \tag{5}$$

Two boundary conditions, the no-slip condition at the wall, and zero shear stress at the free surface and the one additional condition relating the second derivative of velocity at the wall to the film slope are:

$$u\,(x, 0) = 0,$$

$$\frac{\partial u}{\partial v}(x,h) = 0,$$

$$\nu\frac{\partial^2 u}{\partial y^2}(x,0) = g\frac{dh}{dx}. \tag{6}$$

The last condition is from the momentum equation applied at the wall. Inlet and outlet conditions are also to be given.

The equations may be nondimensionalized using the scales used by Bohr *et al*[8]. The length and velocity scales are :

$$x_s = q^{5/8}\nu^{-3/8}g^{-1/8}, \qquad y_s = q^{1/4}\nu^{1/4}g^{-1/4},$$
$$u_s = q^{1/8}\nu^{1/8}g^{3/8}, \qquad v_s = q^{-1/4}\nu^{3/4}g^{1/4}. \tag{7}$$

Then the nondimensional forms of eqns (1) to (5) are :

$$\frac{\partial(ux)}{\partial x} + \frac{\partial(vx)}{\partial y} = 0 \tag{8}$$

$$u\frac{\partial u}{\partial x} + v\frac{\partial u}{\partial y} = \frac{\partial^2 u}{\partial y^2} - \frac{dh}{dx} \tag{9}$$

$$\int_0^1 uxdy = 1 \tag{10}$$

$$\frac{1}{x}\frac{d}{dx}\int_0^h (u^2 x)\, dy = \frac{\partial u}{\partial y}(x,0) - h\frac{dh}{dx} \tag{11}$$

$$\frac{d}{dx}\int_0^h \frac{(u^3 x)}{2} dy = -x\int_0^h \left(\frac{\partial u}{\partial y}\right)^2 dy - \frac{dh}{dy}. \tag{12}$$

The boundary conditions in nondimensional form are accordingly changed. Note that we have retained the same symbols for the nondimensional variables also. Of course, the reduction in the number of parameters is the main advantage in using nondimensional equations. In the present case, the only parameters required are the inlet and outlet conditions. Similar scaling factors may also be derived for certain other types of film flows[17].

3. Watson's solution

In the special case when the gravity term in the momentum equation, (2), is neglected Watson[1] obtained a similarity solution in the fully developed region of the flow (region III). He obtained approximate solutions in regions I and II. In the stagnation region (I) the boundary-layer thickness is of $O(\nu a/U_j)^{1/2}$. In the developing region (II) the boundary layer changed from the Blassius profile to the similarity profile. Watson, however, on the basis that the two profiles are not very different assumed the velocity profile to be the similarity profile for the full length of region II and used the Karman–Pohlhausen method to get the boundary-layer thickness,

$$\delta = 4.58a\sqrt{\frac{\nu x}{Q}}. \tag{13}$$

From continuity the film thickness,

$$h = \frac{a^2}{2x} + \delta = \frac{a^2}{2x} + 1.762a\sqrt{\frac{\nu x}{Q}}. \tag{14}$$

The distance, x_0, at which the boundary layer touches the free surface is then given by,

$$x_0 = 0.315a\, R^{1/3} \tag{15}$$

where $R = Q/\nu a$ is the jet Reynolds number, and the film thickness and the free surface velocity at this point are given by

$$h\,(x_0) = 2.577a\, R^{-1/3} \tag{16}$$

and

$$U\,(x_0) = U_j \tag{17}$$

Instead of Watson's similarity profile if we use the Blassius profile, eqns (13) to (16) are replaced by the following equations

$$\delta = 5.64a\sqrt{\frac{\nu x}{Q}}$$

$$h = \frac{a^2}{2x} + \delta = \frac{a^2}{2x} + 1.941a\sqrt{\frac{\nu x}{Q}}$$

$$x_0 = 0.263\ a\ R^{1/3}$$

$$h\ (x_0) = 2.89\ a\ R^{-1/3}.$$

There is some difference between the two sets of relations. We will, however, use the relations given by Watson in the rest of the paper.

In region (III), Watson assumed a velocity profile of the form $u/U = f(y/h)$, where U is the free surface velocity and obtained the similarity solution. The nondimensional velocity profile can be obtained analytically and expressed in Jacobian elliptic functions .

From the solution we get the relations to calculate the film thickness and the free surface velocity :

$$h^* = \frac{h}{a}R^{1/3} = \frac{3.8}{x^*}\left(x^{*3} + 0.1823\right) \tag{18}$$

$$U^* = \frac{U}{\left(Q/a^2\right)} = \frac{0.068}{0.1823 + x^{*3}}. \tag{19}$$

The nondimensional distance is given by $x^* = (x/a)\ R^{-1/3}$. Expressing the film thickness and the free-surface velocity in the above nondimensional form seems to be natural, and is also used by Azuma *et al*[13].

The initial conditions given by (15)–(17) have been used to calculate the integration constants to obtain (18) and (19).

We, again, remark that Watson's solution is invalid in regions IV, V and VI, where gravity cannot be neglected. As with any similarity solution, Watson's solution is very useful; we can calculate quantities like Reynold's number and Froude number easily for any given set of parameters. It may be noted that no similarity solution is possible when the gravity term is included.

4. Integral methods

A simple albeit approximate solution of the film flow with the gravity term included can be obtained from solving the integral equations (3) and (4) or (10) and (11). Methods based on the Karman momentum integral have been usefully applied to boundary layers (see, for example, Schlichting[18]). To extend the methods to film flows two important differences between film flows and boundary layers should be noted. One difference is due to the gravity terms in the momentum equation. The other difference comes from the fact that volume flux is constant in film flows but continuously increases in the stream

direction because of entrainment in boundary layers (see Arakeri[17] for a fuller discussion). We need to assume a velocity profile; the simplest is a third-order polynomial,

$$\frac{u}{U} = f(\eta) = a\eta + b\eta^2 + c\eta^3 \tag{20}$$

where $\eta = y/h$. The nonslip boundary condition is already satisfied by (20). From the other two conditions in (6) and from $f(1) = 1$ we get

$$b = \frac{h^2}{2\nu u} g \frac{dh}{dx}. \tag{21}$$

In the Polhausen method applied to boundary layers a fourth-order polynomial is used because of the additional condition $\partial^2 u / \partial y^2 = 0$ at the edge of the boundary layer. Equation (20) is rewritten as

$$f(\eta) = \frac{3}{2}\eta - \frac{\eta^3}{2} + b\left(-\frac{\eta}{2} + \eta^2 - \frac{\eta^3}{2}\right) \tag{22}$$

where b is given by (21). The coefficient is similar to the pressure gradient parameter in boundary layers. Some profiles of interest are: $b = 0$ ($dh/dx = 0$), $b = 3$ (separating profile) and $b = -1$ (parabolic). Note that b varies with x and is related to the film thickness and free stream velocity through (21). Integral methods have been applied to film flows in the past, but all have assumed profiles with two constant coefficients satisfying the first two conditions in (6); the third condition has been ignored. The momentum integral equation (4) can be rewritten as

$$\frac{1}{x}\frac{d}{dx}\left(xU^2 h I_2\right) = -\frac{\nu U}{h} f'(0) - gh\frac{dh}{dx}$$

or using (3) as

$$\frac{d}{dx}\left(\frac{UI_2}{I_1}\right) = -\frac{\nu f'(0)}{I_1 h^2} - \frac{g}{UI_1}\frac{dh}{dx}. \tag{23}$$

Here $I_n = \int_0^1 f^n d\eta$ and $I_n = \int_0^1 (f')^n d\eta$ and are functions of b. Values of the relevant integrals, for various values of b, are listed in Table I.

Table I

Values of constants for various velocity profiles

b	I_1	I_2	I_2'	I_3	I_2/I_1	*Velocity Profile*
−1.0	0.67	0.53	1.13	0.45	0.79	Parabolic
0.0	0.625	0.49	1.2	0.4	0.78	Zero pressure gradient
1.0	0.58	0.44	1.13	0.37	0.76	Adverse pressure gradient
2.0	0.54	0.405	1.13	0.335	0.75	Adverse pressure gradient
3.0	0.50	0.37	1.2	0.3	0.74	Separating

Note that the quantities involving integrals do not vary much but the quantity $f''(0) = a = 3/2 - b/2$ varies between 2 and 0 for the values of b given in the table. Using (22) we get $f'(0) = 3/2 - 1/4\ h^2/\nu Ug\ dh/dx$. Substituting for $f'(0)$ in (23) we get

$$\frac{d}{dx}\left(\frac{UI_2}{I_1}\right) = -\frac{3}{2} - \frac{3}{4}\frac{g}{UI_1}\frac{dh}{dx}. \tag{24}$$

Now, all the quantities related to b (*i.e.*, I_2/I_1 and I_1) are slowly varying functions. We have unknowns h, U and b and three equations: momentum (24), mass conservation (3) and the boundary condition (21). These equations are nonlinear but can be solved iteratively.

The energy integral equation can be written as

$$\frac{d}{dx}\left(\frac{U^3}{2}xhI_3\right) = -\nu x\frac{U^2}{h}I_2' - gq\frac{dh}{dx}$$

or

$$\frac{d}{dx}\left[\frac{U^2}{2}\frac{I_3}{I_1}\right] = -\nu\frac{U}{h^2}\frac{I_3'}{I_1'} - g\frac{dh}{dx}. \tag{25}$$

Equation (25) is like the Bernoulli equation with the first term on the right-hand side representing frictional loss.

It is useful to assume the integrals, I_n are constants and write the equations as a single equation

$$\frac{dh}{dx} = \frac{\dfrac{-f'(0)}{q}\dfrac{I_1}{I_2}x + \dfrac{h}{x}}{\dfrac{x^2gh^3}{q^2}\dfrac{I_1^2}{I_2} - 1}$$

or substituting for $f'(0)$ as before we get

$$\frac{dh}{dx} = \frac{\dfrac{3}{2Re_hI_2}\dfrac{h}{x}}{1 - \dfrac{3}{4I_2Fr_h}} \tag{26}$$

where $Re_h = Uh/\nu = q/\nu\ x\ I_1$ and $Fr_h = U^2/gh = q^2/gh^3\ x^2\ I_1^2$.

We should remember the two important assumptions in arriving at (26): the velocity profile is cubic and thus $f'(0) = 3/2 - 1/4\ h^2/\nu\ Ug\ d\ dh/dx$ and I_1 and I_2 are constants. We gain further insight, however, by studying (26) rather than the earlier more exact

equations. The gravity term is represented by the second term in the denominator; neglecting this term is Watson's approximation and we can solve (26) exactly to recover (18) and (19) but with different values of the constants. Equation (7) tells us that gravity can be neglected (Watson's solution is valid) as long as $1/I_2\ Fr_h << 1$, *i.e.*, large local Froude numbers.

In open channel hydraulics, an equation similar to (26) is obtained except for the term (h/x) in the numerator which is due to radial flow. Depending on the signs of the denominator and numerator dh/dx may be positive or negative. Near Froude number unity we have a singularity. We note in the inviscid limit, $Re_h \to \infty$, the film thickness increases with x for Froude number less than unity and *vice versa*.

5. Jump and edge conditions

If a hydraulic jump occurs then we need two more conditions to solve the problem: the jump condition and the condition at the edge of the plate ($x = R_p$).

The jump condition is easily derived by applying the continuity and momentum equation across the hydraulic jump. The condition for uniform upstream and downstream flows and without friction at the wall was derived by Lord Rayleigh and is given in standard fluid-mechanics textbooks. For nonuniform velocity profiles and a finite jump extent in the flow direction we get[19],

$$H^3 - H\left(2Fr\,I_2 + 1 + D\right) = 2Fr\,I_2\,\frac{I_2'}{I_2}\,\frac{I_1}{I'^2} = 0 \tag{27}$$

where $Fr = U^2/gh$, $H = h'/h$ and $D = 2\,\tau_w\,X/(\rho g h^2)$.

The primed quantities refer to downstream of the jump and nonprimed quantities to upstream of the jump. τ_w is the wall shear stress and X, the length of the jump. The effect of nonuniform velocity profiles enters through the integrals I_1, I_2, etc. We recover Rayleigh's result if the integrals are unity and $D = 0$. For $D = 0$, we may solve (27) to get the height ratio

$$H = \frac{h'}{h} = \frac{1}{2}\sqrt{1 + \frac{8\,Fr I_2}{I_1^2}}. \tag{28}$$

Note that a separation bubble in the jump region would imply that $\tau_w > 0$.

In hydraulics the edge condition is assumed to correspond to minimum energy (which corresponds to unity Froude number). This condition also implies that no waves propagate upstream from downstream of the edge. We follow the same principle. The energy equation is

$$\frac{d}{dx}\left[\frac{U^2}{2}\left(\frac{I_3}{I_1}\right)\right] = -\nu\,\frac{U}{h^2}\,\frac{I_2'}{I_1} - \frac{1}{q}\int_0^h \frac{\partial p}{\partial x}\,u\,dy. \tag{29}$$

Consider the edge to be of varying slope with the surface making an angle α with the horizontal and with the local radius of curvature given by R. Surface tension and centrifugal forces are important if the radius of curvature is small. The pressure obtained by integrating the y momentum equation is

$$P(x,y) = P_\sigma - \rho g \cos\alpha \, y \,||\, {}_h^y + \int_h^y \frac{\rho u^2}{R+y} dy. \tag{30}$$

The first term is pressure due to surface tension and is approximately given by

$$P_\sigma = \frac{\sigma}{R+h}. \tag{31}$$

The simple addition of h to R to get the free surface radius of curvature is the approximation. The second term is the hydrostatic term; the third is due to centrifugal acceleration where it is assumed that the streamlines are parallel to the surface.

Substituting for dp/dx using (31) in (30) and neglecting the centrifugal term we get

$$\frac{d}{dx}\left[\frac{U^2}{2}\frac{I_3}{I_1} + g\cos\alpha\, h + \frac{\sigma}{\rho(R+h)}\right] = -\nu\frac{U}{h^2}\frac{I_2'}{I_1} + g\sin\alpha. \tag{32}$$

The term within the brackets on the left-hand side is like the specific energy used in open channel hydraulics and is to be minimized to get the critical condition. Assuming $h/R << 1$, the critical height becomes

$$h_{cr} = \frac{Q(2/3)\left(I_3/I_1^3\right)^{1/3}}{\left(g\cos\alpha - \left(\sigma/\rho R^2\right)\right)^{1/3}}. \tag{33}$$

For $\sigma = 0$ (33) corresponds to the well-known unity Froude number condition. We see that for convex surfaces the effect of surface tension is to increase the critical height. The definition of edge becomes unclear when the plate has a smoothly varying curve near the end of the plate. Recently, Higuera[20] has derived the structure of the flow near the edge of the plate.

6. Results from the integral method

Now we have all the equations and boundary conditions to solve the radially spreading thin film flow. We present results for a specific case of a water jet with $Q = 3$ lpm, $a = 0.5$ cm and plate radius $R_p = 20$ cm. Values of the corresponding nondimensional parameters are $R = 10{,}000$ and $Fr = U_j^2/g\,a = 8.27$. Film height at the edge of the plate is obtained from (32) with surface tension neglected. The supercritical region of the flow is obtained by marching downstream from the jet impingement point. The subcritical region is obtained by marching upstream from the edge of the plate. The two solutions can be connected by fitting a hydraulic jump.

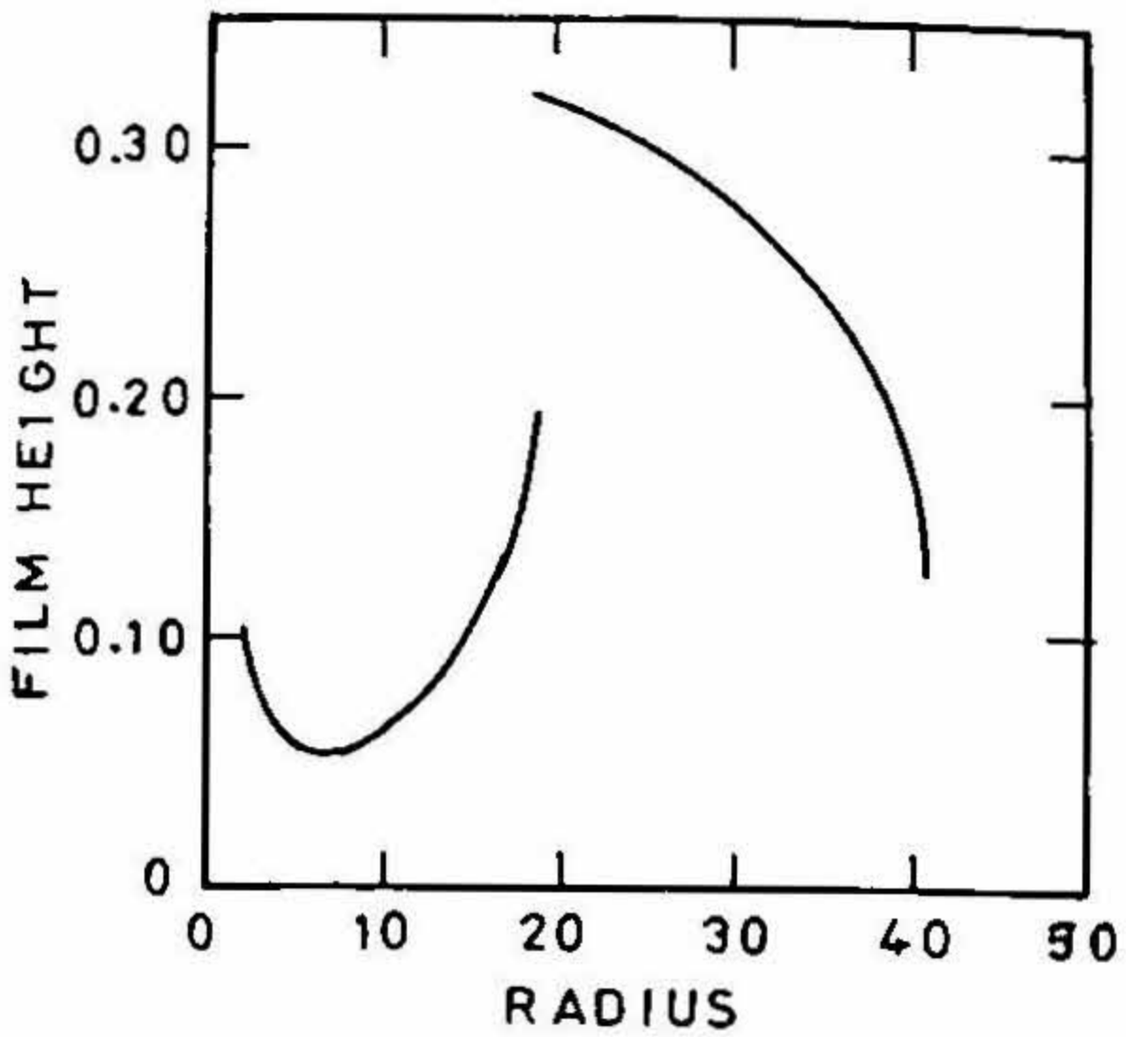

FIG. 2. Computed film thickness nondimensionalized by jet radius *versus* radius Q = 3 lpm, jet radius = 0.5 cm.

The film thickness initially decreases and then increases in the supercritical region; in the subcritical region, the film thickness continuously decreases (Fig. 2). The initial decrease can be explained from (27) as due to the 'axisymmetric term' (For plane flows this term is absent and thickness increases downstream for supercritical flows.).

The surface velocity nondimensionalized by the jet velocity is shown in Fig. 3. The local Reynolds number continuously decreases with distance (Fig. 4), by a factor of almost ten over the radius of the plate. There is a large reduction in the Froude number in the supercritical region of the flow (Fig. 5a). Note the rapid approach to unity Froude number near the edge of the plate (Fig. 5b).

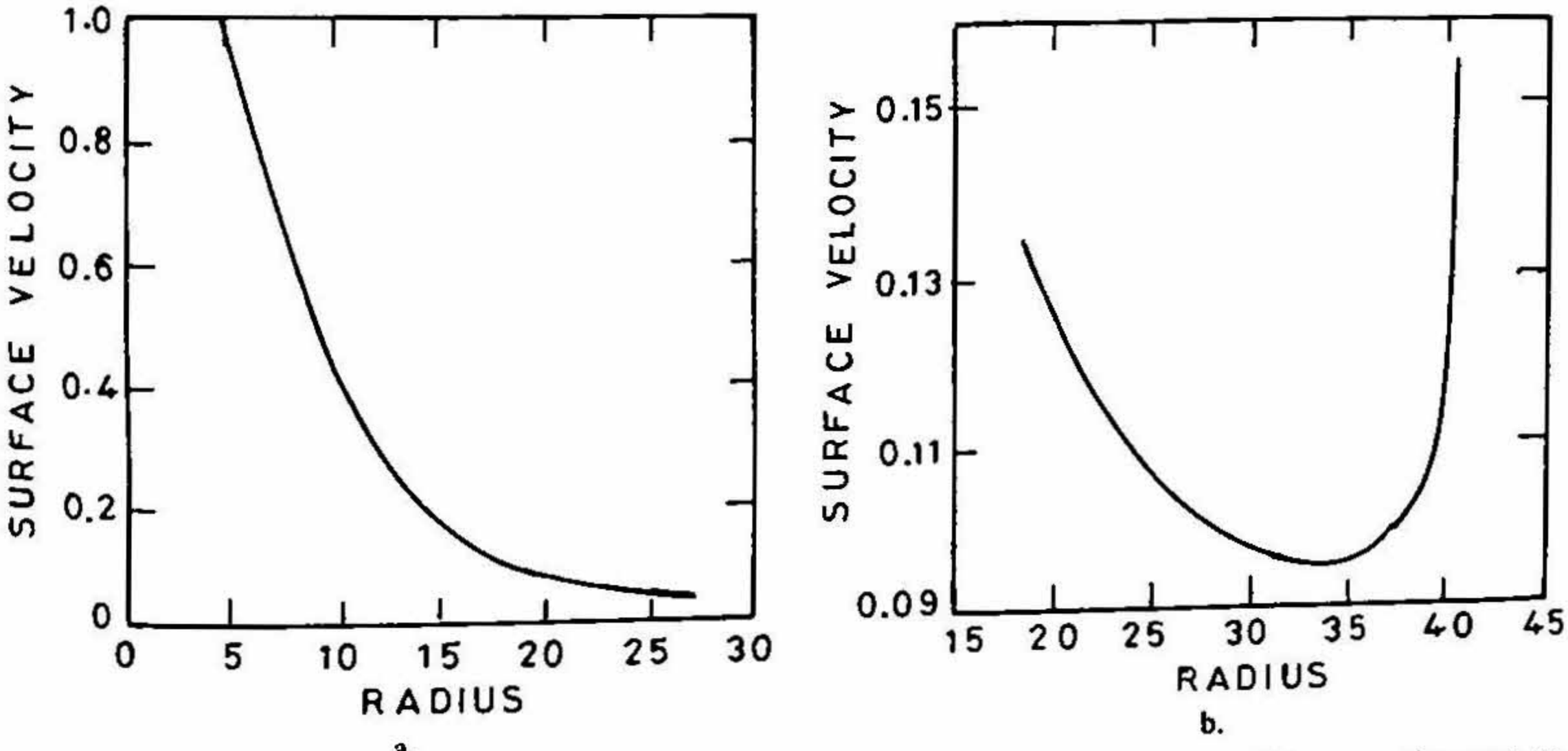

FIG. 3. Computed surface velocity nondimensionalized by jet velocity *versus* radius. Conditions are the same as in Fig. 2; a) upstream and b) downstream of the jump.

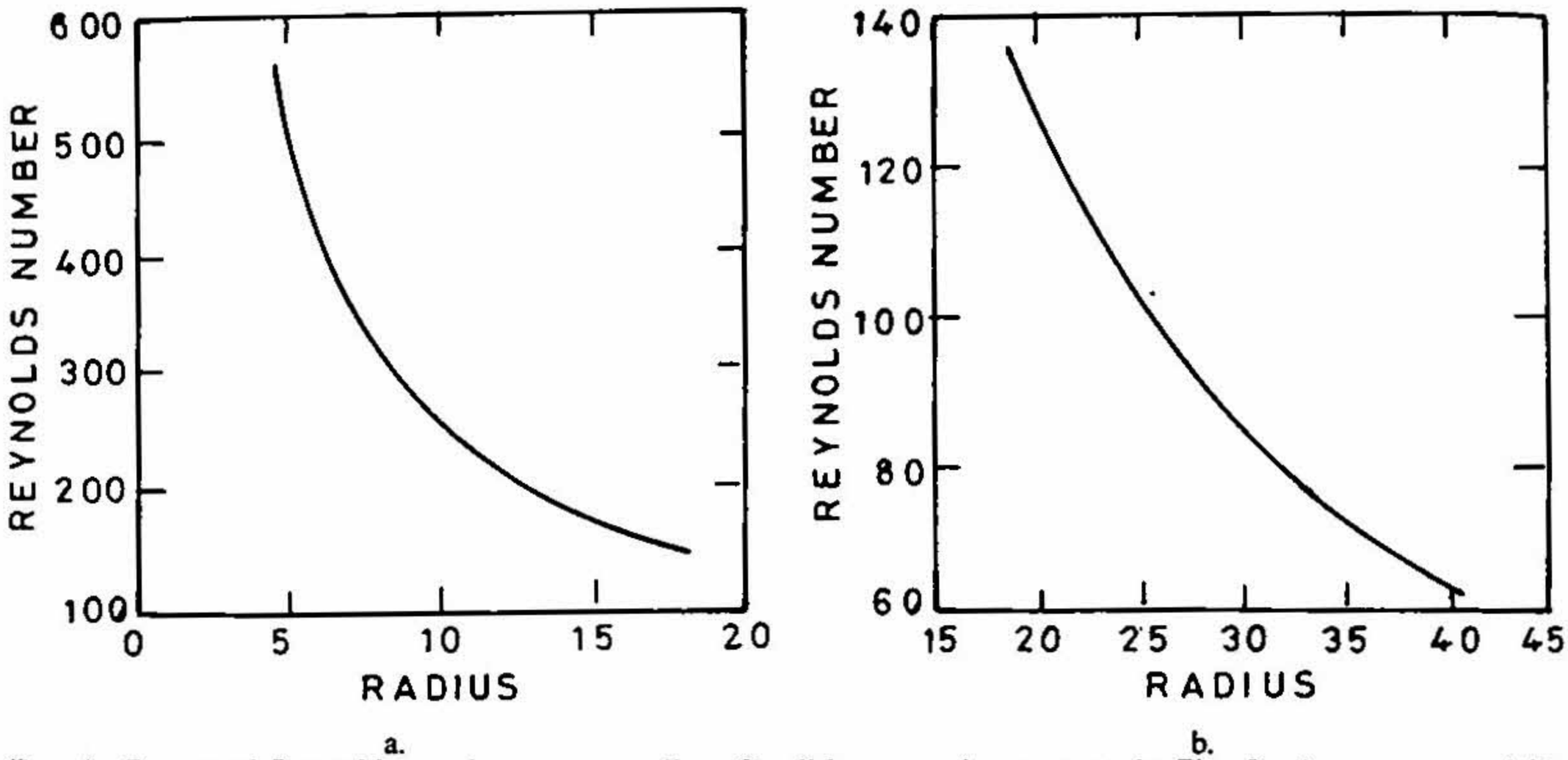

FIG. 4. Computed Reynolds number *versus* radius. Conditions are the same as in Fig. 2; a) upstream and b) downstream of the jump.

The rapid increase of film thickness near $r/a = 17$ is due to the combined effect of viscosity and the adverse pressure gradient term $-g\ dh/dx$. This point corresponds to where Fr is 0 (1), *i.e.*, at the point where gravity becomes important. We may thus expect Watson's solution to deviate from our solution at $r/a \approx 17$ which indeed is the case (Fig. 6). The variation of the coefficient b (see eqn 21) is interesting (Fig. 7). In the region where $Fr >> 1$ ($r/a < 16$) $b \approx 0$ (zero pressure gradient flow). The separation point ($b = 3$ is predicted at $r/a \approx 18$). The relationship between separation and the hydraulic jump, if any, is hard to tell. Clearly we can have flows with a hydraulic jump upstream of the separation point, for example, by having a barrier at the edge of the plate. It is not, however, clear whether a separation bubble can be obtained without a

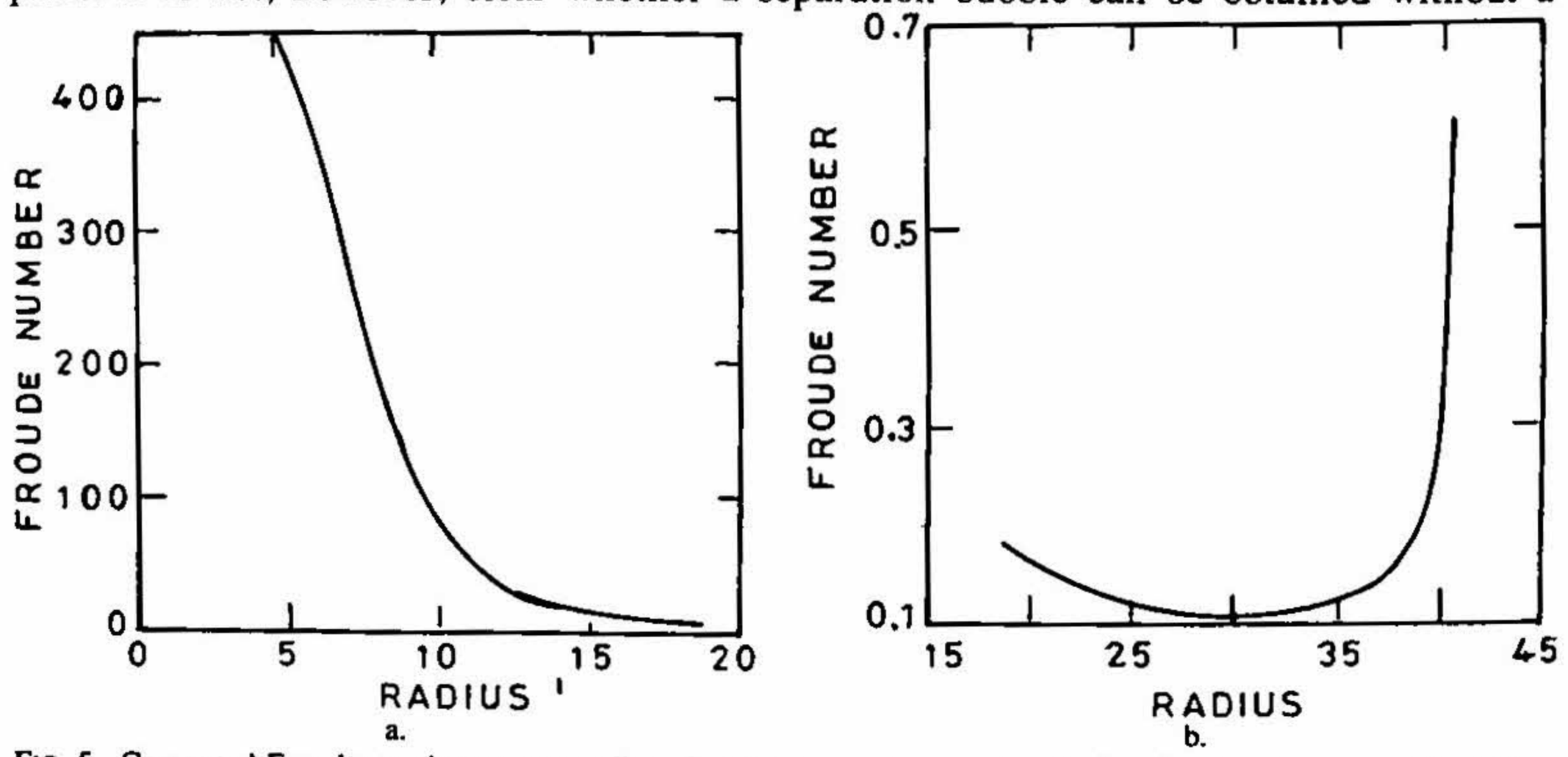

FIG. 5. Computed Froude number *versus* radius. Conditions are the same as in Fig. 2; a) upstream and b) downstream of the jump.

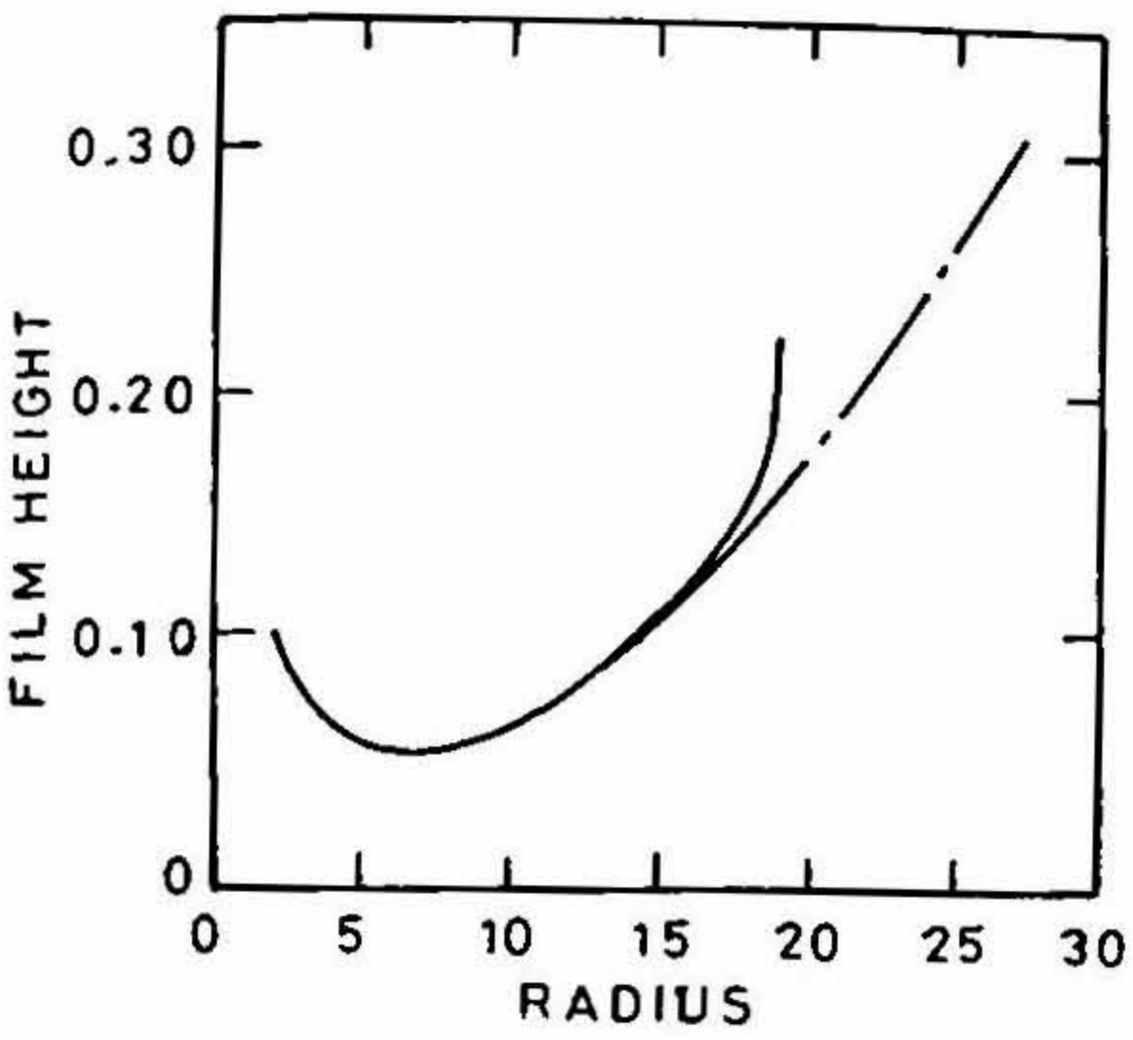

FIG. 6. Figure showing difference between the integral method calculation (full line) and Watson's solution (dash-dotted line).

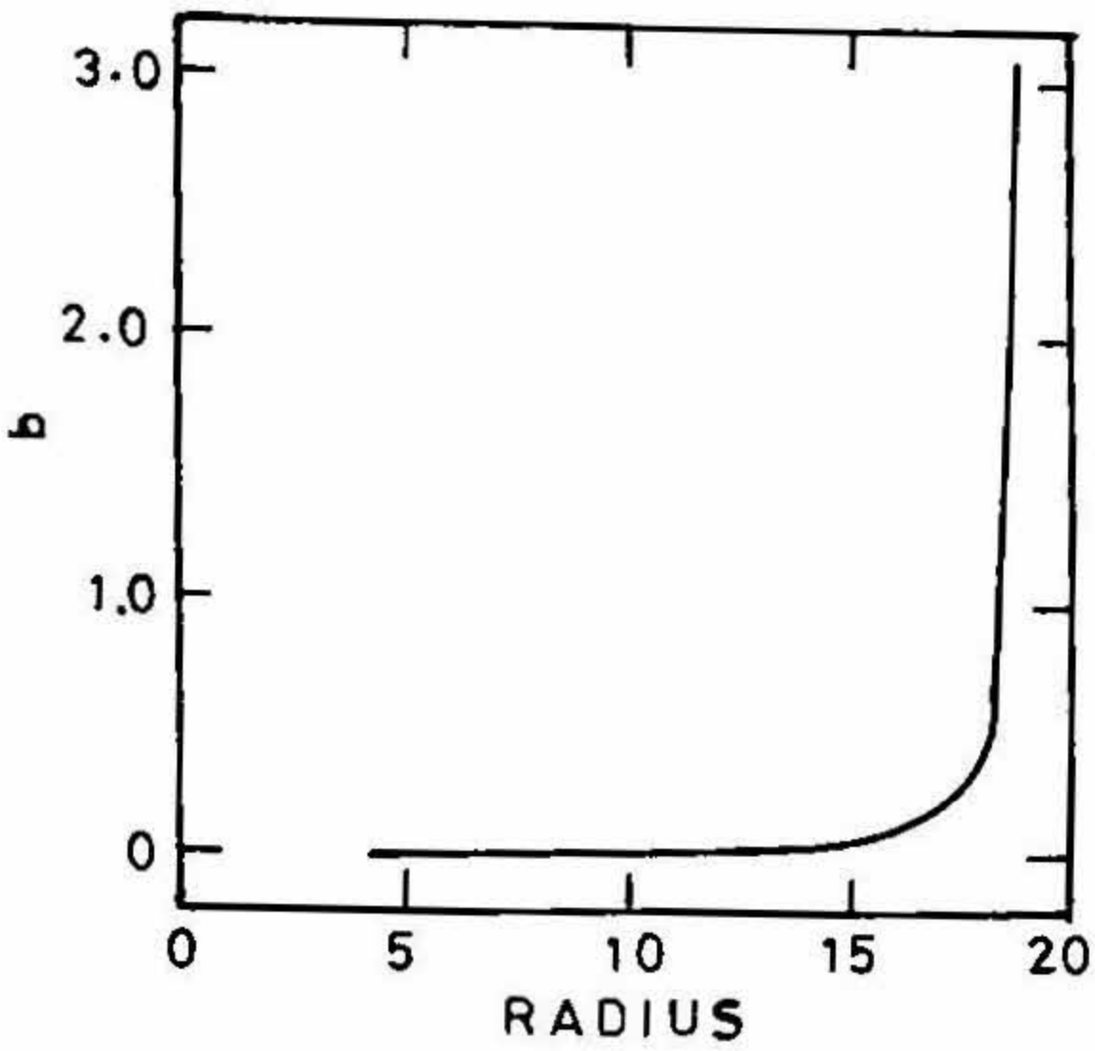

FIG. 7. Variation upstream of the jump of the coefficient b in the polynominal for the velocity profile.

hydraulic jump. Finally, we note that prediction of the separation point using integral methods is possible only by the method we have proposed, *i.e.*, by allowing the shape of the velocity profile to change, *i.e.*, by having the coefficient b as variable.

7. Experimental results

In this section, we briefly present some experimental results. The setup consists of a nozzle with exit radius $a = 0.5$ cm, an overhead tank, 1/4 hp centrifugal pump and a rotameter. The plates on which the jet impinged were either made of aluminium or glass and were of various diameters. The flow rate was varied between 1 and 15 lpm. Details are available in Achuth Rao[19].

7.1. *Film thickness measurements*

Film thickness was measured using a simple conductivity probe: a sewing needle traversed vertically indicated contact with water by a sudden drop in electrical resistance between the needle and the aluminium plate and contact with the plate by another drop in resistance. The difference in the heights of the two drops in resistance gives the film thickeness. Figure 8 shows the film thickness variations for a flow rate of 2 lpm for 20- and 30-cm diameter plates. Solution using the integral method compares well upstream of the jump but downstream the difference between the computed and the measured values is as much as 50%. We presume that this error is because the edge condition used to calculate the results of Fig. 8 is wrong. The edge of the plate used in the experiments is curved and this has not been accounted for in the edge height calculation; also surface tension has been neglected, inclusion of which would increase the critical height (see eqn 33), though, marginally in the present case.

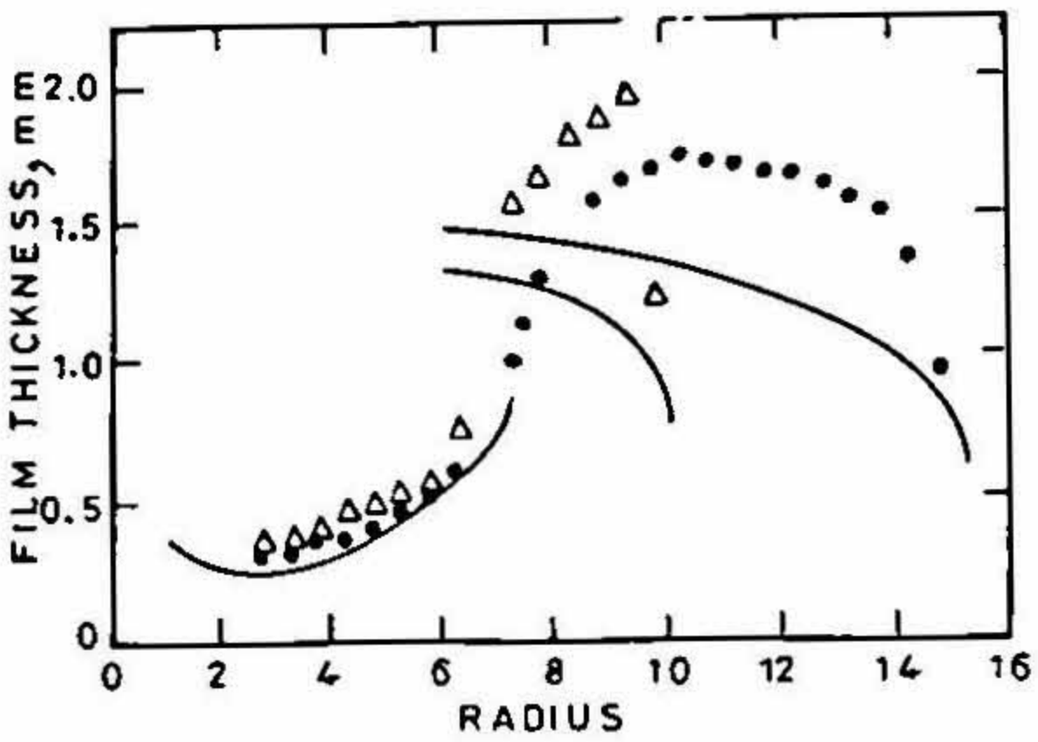

FIG. 8. Comparison of measured and computed film thickness up and downstream of the jump. Q = 2 lpm, nozzle height = 15 cm, a = 0.5 cm Δ plate diameter =20.5 cm. • plate diameter = 30.6 cm.

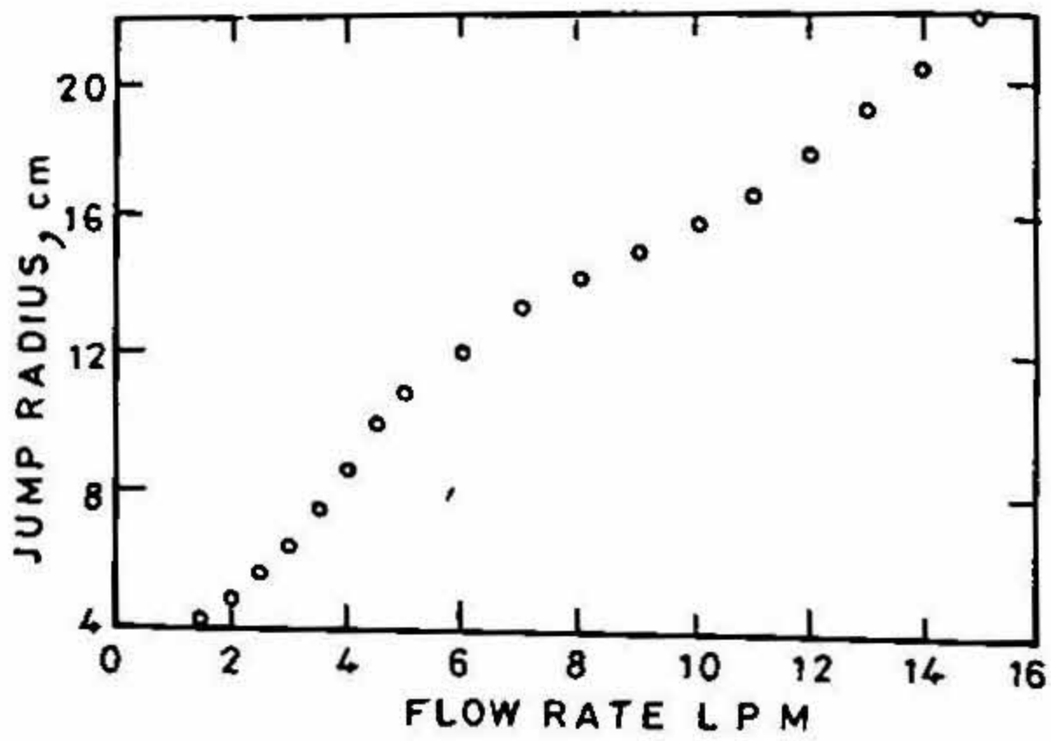

FIG. 9. Measured hydraulic jump radius *versus* flow rate. Diameter of the glass plate = 61 cm.

7.2. *Jump location*

The hydraulic jump location is plotted *versus* flow rate in Fig. 9 for the jet impinging on the 61-cm-diameter glass plate. The jump location continuously moves downstream with flow rate with an apparent change in slope at around Q = 5 lpm. This was also the flow rate at which transition to turbulence was observed. Bohr *et al.*[8]'s prediction of jump location for large plates agrees well for the lower flow rates. Interestingly, calculating the position of breakdown of Watson's solution say at Fr = 10, we obtain the same scaling as that of Bohr *et al.*[8]

Breakdown of Watson's solution also indicates the point at which gravity becomes important and just downstream separation is to be expected. Thus it appears that the jump location for flows without a barrier is very close to the separation point.

7.3. *Flow visualization*

Figure 10 shows a series of photographs visualizing the flow at flow rates from 2 to 15 lpm due to jet impingement on the 61-cm glass plate. The photographs show shadow pictures on a white sheet of paper stuck to the bottom surface of the glass plate with lighting from a 1000 W halogen lamp placed about 30° to the horizontal and the camera looking vertically down. The height of the nozzle was 15 cm from the glass plate (Fig. 11).

7.3.1. *Waves downstream of the jump*

At flow rates less than about 4 lpm waves the flow is laminar. The jump location is steady at very low flow rates (<1 lpm) but unsteady at the higher flow rates. We observe axisymmetric waves downstream of the jump (Fig. 10a–b); they are more prominent at higher flow rates. They do not seem to be periodic but seem to come in packets. Calculation shows that the group velocity is greater than the phase velocity for the conditions

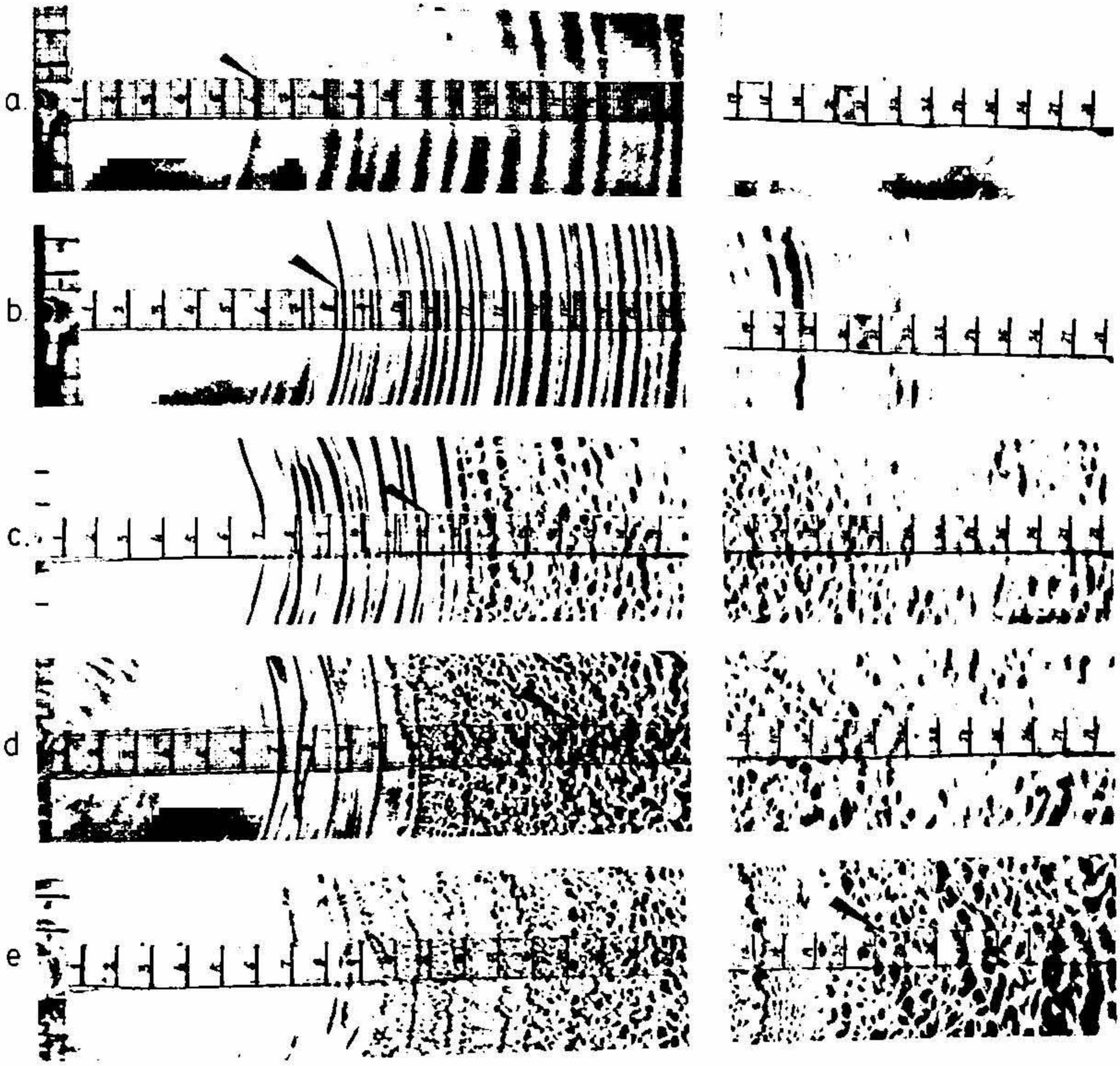

FIG. 10. Shadowgraph pictures of the film for several flow rates. The left-hand set of pictures are for x = 0-16 cm and the right-hand set are for x = 16 to 29 cm. The hydraulic jump location is marked by the dark triangles. a) $Q = 2$, b) $Q = 4$, c) $Q = 6$, d) $Q = 10$, e) $Q = 15$ lpm.

obtained in our experiments. We thus would expect these waves to be dispersive and, as pointed out by Craik *et al.*[10], they cannot be stationary. (To get standing waves the phase velocity should be greater than the phase velocity as in the cnoidal waves downstream of a hydraulic jump in not-thin-film flows[21].) The waves, therefore, must be produced by an unsteady source presumably at the jump. Our attempts to measure the phase speed of the wave and the frequency of excitation of this unsteady source by the needle method were inconclusive. At the higher flow rates, the waves are no longer axisymmetric but this could be due to the 'source' at the jump itself becoming non-axisymmetric because instability of the flow at the jump.

7.3.2. *Waves upstream of the jump*

For flow rates greater than about 4 lpm, we observe concentric waves upstream of the jump. They seem to appear suddenly at some radial distance, at least, at lower flow rates. These waves, we believe, have their origin in the Rayleigh instability of the liquid jet before it impinges on the plate. The 15-cm nozzle height allows the instability to grow and manifest itself as undulations propagating at $u + c$ on the film surface; here c is the wave phase speed. If the undulations are large enough they can grow and break. This, presumably, is the reason for the fairly 'sudden' appearance of the waves: the undulations though present right from the point of impingement appear in the shadow pictures only after they have grown to sufficient magnitude. The distance between the waves is equal to the propagation velocity (at $u + c$) multiplied by the time period of the waves on the jet and thus it reduces with downstream distance as clearly seen in Fig. 10c.

The relationship between the upstream waves and the waves on the jet needs to be conclusively established. That the jet does indeed have undulations is clearly seen in Fig. 11. We are, however, still not certain whether the origin of the waves is in the jet or in an instability of the film flow itself. Azuma *et al.*[12] observed similar waves even though in their case the nozzle was very close to the plate surface. They call these waves roll waves in analogy to the ones found on inclined plane film flows. When we reduced the distance of the nozzle from the plate to 1 cm the waves (upstream of the jump) appeared further downstream but were not completely eliminated at the higher flow rates (compare Figs 10 and 12).

7.4. *Transition and turbulence*

There are two important aspects to transition to turbulence of radially spreading film flows. One is that the Reynolds number is maximum at the point at which the boundary layer touches the free surface (end of region II in Fig. 1) and goes down like the inverse of radial distance (see Fig. 4). The other aspect is related to the fact that in region IV (where the pressure gradient is adverse) and in the hydraulic jump region the velocity profiles have inflection points; such profiles are very unstable. Thus, transition may occur due to the instability of the Watson profile in region III or due to the instability of the inflection-point profiles in regions IV and V.

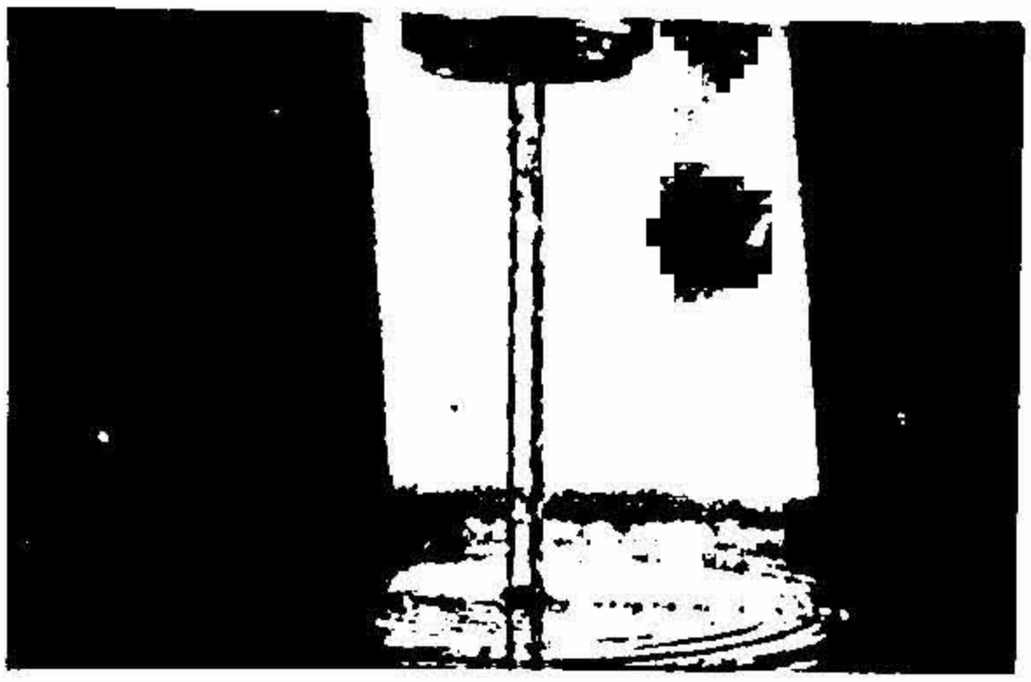

FIG. 11. Photograph showing the surface waves on the impinging jet.

FIG. 12. Transition in the absence of surface waves. $Q = 15$ lpm.

Azuma *et al.*[16] have observed and studied the transition in region III, *i.e.*, instability of the Watson profile. Using Watson's solution, we get the local Reynolds number

$$Re_h = \frac{uh}{\nu} = 0.258 \frac{R^{2/3}}{r^*} \tag{34}$$

which is maximum at x_0 and is

$$Re_{h\max} = 0.819 R^{2/3}. \tag{35}$$

The critical Reynolds number for Watson's profile is $Re_{hcr} = 450$. Experimentally, Azuma *et al.* found that transition occurred for the jet Reynolds number exceeding 7.4×10^4. The transition point was at $r^* = 0.65$ at $R = 7.4 \times 10^4$ and moved upstream like $R^{-2/3}$ with increase in the jet Reynolds number. At $R = 7.4 \times 10^4$ the local Reynolds number (Re_h) at the transition point was 470. We note that for all the cases the instability and transition is in the region where Watson's solution is valid.

In the presence of surface waves, as in our case, the transition process gets altered dramatically. We observe transition to turbulence first at a flow rate of about 5 lpm ($R = 1.7 \times 10^4$). The breakdown occurs at about the same location as the hydraulic jump 5 lpm (Fig. 10). The local Reynolds number is about 210 at this location, much lower than the critical Reynolds number of Watson's profile. Clearly the transition is due to the instability of the inflection point profiles at the jump.

At 10 lpm transition occurs at about 11 cm, where the local Reynolds number is about 390. The maximum Reynolds number is calculated to be 870 at $r = 5$ cm. We do not, however, observe transition at the maximum Reynolds number location but do so further downstream. The reason for this is probably that waves have to grow (which they do as they travel downstream) to a certain amplitude before they cause transition. The jump occurs at 16 cm and it is interesting to note the clear change of scale in the turbulence across the jump.

At the highest flow rate we have studied 15 lpm, ($R = 5 \times 10^4$) the transition is again wave induced and occurs at about 10 cm, where $Re_h = 645$. Note again that there is no sign of breakdown at the maximum Re_h location which in this case is at $r = 5.8$ cm. Another curious fact is the existence of waves till the hydraulic jump at around 20 cm even after the breakdown to turbulence. The change in scale of the turbulence across the jump is again observed.

The surface wave-induced transition needs further discussion. The wave seems to modify the local velocity profile sufficiently so that transition is triggered. The transition is initiated in the form of longitudinal streaks scaling probably with the local thickness (see Fig. 10). The propagation velocity ($U + c$) of the wave is greater than the fluid velocity; thus, the wave triggers transition and leaves the turbulence behind (An analogous situation is a shock wave-induced transition in gas-flow boundary layers.). If the local Reynolds number is high enough (close to the critical value) then turbulence should be sustained at least for some distance. We may expect relaminarization but do not know

whether it has set in the flows we have studied. For example, in the 10 lpm flow the Reynolds number at the jump is about 280 which is lower than the critical value.

To visualize transition in the absence of waves, we reduced the nozzle distance to 1 cm (Fig. 12). The waves are of much lower amplitude and the transition mechanism seems to be similar to that observed by Azuma *et al.*

8. Conclusion

In this paper, we have looked at a radially spreading film flow at high Reynolds numbers. This flow has many interesting features related to wave phenomenon, hydraulic jumps, free surface flows and transition. We have discussed the new integral method (with variable coefficients) applicable to film flows. We find that capillary waves induced in the impinging jet amplify in the film flow. These waves can induce transition to turbulence. The dynamics of these waves need further study.

References

1. WATSON, E. J — The radial spread of a liquid over a horizontal plane, *J. Fluid Mech.*, 1964, 20, 481–499.
2. TANI, I. — Water jump in the boundary layer, *J. Phy. Soc. Jap.*, 1949, 4, 212–215.
3. BUYEVICH, YU. A. AND USTINOV, V. A., — Hydrodynamic conditions of transfer processes through a radial jet spreading over a flat plate, *Int. J. Heat Mass Transfer*, 1994, 37, 165–173.
4. THOMAS, S., FAGHRI, A., HANKEY, W. L., AND SWANSON,T. D. — One dimensional analysis of the hydrodynamic and thermal characteristics of thin film flows including the hydraulic jump and rotation, *J. Heat Transfer*, 1990, 112, 728–735.
5. RAHMAN, M. M., FAGHRI, A., HANKEY, W. L. AND SWANSON, T. D. — Computation of the free surface flow of a thin liquid film at zero and normal gravity, *Num. Heat Transfer A*, 1990, 17, 53–71.
6. RAHMAN, M. M., HANKEY, W. L. AND FAGHRI, A. — Analysis of the fluid flow and heat transfer in a thin liquid film in the presence and absence of gravity, *Int. J. Heat Mass Transfer*, 1991, 34, 103–114.
7. RAHMAN, M. M., FAGHRI, A. AND HANKEY, W. L. — Computation of turbulent flow in a thin liquid layer of fluid involving a hydraulic jump, *J. Fluid Engng*, 1991, 113, 411–418.
8. BOHR, T., DIMON, T. AND PUTKARADZE, V. — Shallow water approach to the circular hydraulic jump, *J. Fluid Mech.*, 1993, 245, 635–648.
9. RAYLIEGH, LORD — On the theory of long waves and bores, *Proc. R. Soc. Lond. A*, 1914, 90, 324–328.
10. CRAIK, A. D. D. — The circular hydraulic jump, *J. Fluid Mech.*, 1981, 112, 347–362.
11. BOWLES, R. I, AND SMITH, F. T. — Standing hydraulic jump:Theory, computation and comparison with experiments, *J. Fluid Mech.*, 1992, 242, 145–168.
12. AZUMA, T. AND HOSHINO, T. — The radial flow of a thin liquid film (1st Report, Laminar turbulent transition), *Bull. JSME*, 1984, 27, 2739–2746.
13. AZUMA, T. AND HOSHINO, T. — The radial flow of a thin liquid film (2nd Report, Liquid film thickness), *Bull. JSME*, 1984, 27, 2747–2754.

14. AZUMA, T. AND HOSHINO, T. The radial flow of a thin liquid film (3rd Report, Velocity profile), *Bull. JSME*, 1984, 27, 2755–2762.

15. AZUMA, T. AND HOSHINO, T. The radial flow of a thin liquid film (4th Report, Stability of liquid film and wall pressure fluctuations), *Bull. JSME*, 1984, 27, 2763–2770.

16. AZUMA, T. AND WAKIMOTO, T. Laminar-turbulent transition of thin radial liquid film flow, *Proc. Third World Conf. on Experimental Heat Transfer, Fluid Mechanics and Thermodynamics*, 1993 (Kelleher *et al.* (eds)), Elsevier Science Publishers, 1993, pp. 936–942.

17. ARAKERI, J. H. Integral methods and scale factors for certain 2-D film flows (under preparation).

18. SCHLICHTING, H. *Boundary layer theory*, 7edn, 1979, McGraw-Hill.

19. ACHUTH RAO, K. P. *Thin film flows: Integral methods and experiments on the circular hydraulic jump*, M.Sc. (Engng) Thesis, Indian Institute of Science, Bangalore, India, 1994.

20. HIGUERA, F. G. The hydraulic jump in a viscous laminar flow, *J. Fluid Mech.*, 1994, 274, 69–92.

21. LIGHTHILL, M. J. *Waves in fluids*, 1978, Cambridge University Press.